Eur. Phys. J. D (2017) 71: 179
DOI: 10.1140/epjd/e2017-80067-0

THE EUROPEAN PHYSICAL JOURNAL D

Regular Article

Dissipation and energy balance in electronic dynamics of Na clusters*

Marc Vincendon[1,2], Eric Suraud[1,2], and Paul-Gerhard Reinhard[3,a]

[1] Institut für Theoretische Physik, Universität Erlangen, 91058 Erlangen, Germany
[2] Université de Toulouse, UPS, Laboratoire de Physique Théorique (IRSAMC), 31062 Toulouse, France
[3] CNRS, LPT (IRSAMC), 31062 Toulouse, France

Received 31 January 2017 / Received in final form 10 May 2017
Published online 4 July 2017 –

Abstract. We investigate the impact of dissipation on the energy balance in the electron dynamics of metal clusters excited by strong electro-magnetic pulses. The dynamics is described theoretically by Time-Dependent Density-Functional Theory (TDDFT) at the level of Local Density Approximation (LDA) augmented by a self interaction correction term and a quantum collision term in Relaxation-Time Approximation (RTA). We evaluate the separate contributions to the total excitation energy, namely energy exported by electron emission, potential energy due to changing charge state, intrinsic kinetic and potential energy, and collective flow energy. The balance of these energies is studied as function of the laser parameters (frequency, intensity, pulse length) and as function of system size and charge. We also look at collisions with a highly charged ion and here at the dependence on the impact parameter (close versus distant collisions). Dissipation turns out to be small where direct electron emission prevails namely for laser frequencies above any ionization threshold and for slow electron extraction in distant collisions. Dissipation is large for fast collisions and at low laser frequencies, particularly at resonances.

1 Introduction

Time-Dependent Density-Functional Theory (TDDFT) is starting point and leading tool to simulate the dynamics of many-fermion systems, in electronic systems [1–3] as well as in nuclei [4–6]. The Local Density Approximation (LDA) provides a robust and efficient mean-field description of dynamics which allows to cover a huge range of phenomena from the linear regime of small-amplitude oscillations (also known as random-phase approximation) [7] to systems possibly highly excited by strong laser pulses [8,9] or hefty collisions [10,11]. However, more detailed observations and/or long-time evolution is often sensitive to all sorts of many-body correlations beyond the mean-field approach [12]. A particularly important class are dynamical correlations from two-fermion collisions. They add dissipation to the mean-field motion which has important consequences in a great variety of dynamical scenarios and systems, e.g., for collisional broadening of excitation spectra [13], for necessary thermalization steps in nuclear reactions [14–16], for thermalization in highly excited electronic systems [17,18]. Dissipation (and thermalization) is a particularly important and much discussed process in the electronic dynamics of small metal clusters [18–22] and plays a crucial role in the quest for most gentle ionization and appearance sizes [23–25]. In the present paper, we address dissipation and energy transport in small metal clusters taking up an affordable approach to dissipation, the Relaxation-Time Approximation (RTA), which had been implemented recently for simulations of finite electronic systems [26].

Although highly desirable, theoretical investigations of dissipation in finite fermion systems have been hampered so far by the enormous computational demands for a microscopic description of two-body collisions in the quantum regime. The way from the full many-body hierarchy down to a mean-field description augmented by dynamical correlations has been thoroughly developed since long in classical non-equilibrium thermodynamics [27], leading eventually to the much celebrated Boltzmann equation to account for dynamical correlations in classical systems [28]. A manageable scheme for a fully quantum mechanical description in finite systems is still a matter of actual research. One important quantum feature is the Pauli principle. It can be accounted for by extending the Boltzmann collision term to the Boltzmann-Uehling-Uhlenbeck (BUU) form [29]. This semi-classical BUU approach (also known as Vlasov-Uehling-Uhlenbeck (VUU) equation) provides an acceptable picture at sufficiently large excitations where quantum shell effects can be ignored. It has been extensively used in nuclear physics [30,31] and also employed for the description of metal clusters in a high excitation domain [32,33]. Although very successful, BUU/VUU is valid only for sufficiently high excitation energies. And even in this domain,

* Contribution to the Topical Issue "Dynamics of Systems at the Nanoscale", edited by Andrey Solov'yov and Andrei Korol.

[a] e-mail: paul-gerhard.reinhard@physik.uni-erlangen.de

de-excitation by ionization can quickly evacuate large amounts of excitation energy thus cooling the system down into a regime where quantum effects count again. In any case, there is an urgent need for a quantum description augmented by relaxation effects.

Such dissipative quantum approaches are still well manageable in bulk systems and have been extensively studied in the framework of Fermi liquid theory [34]. It was found that global features of dissipation can often be characterized by one dominant, exponential relaxation mode. This motivated the Relaxation Time Approximation (RTA) as was introduced in [35] and later on applied to a wide variety of homogeneous systems [36,37]. The quantum case for finite systems is much more involved. A full description of detailed correlations has been carried through in schematic model systems [38] and in the time-dependent configuration-interaction (TD-CI) method [39], both being limited to simple systems. A stochastic treatment of the quantum collision term promises a tractable approach [40]. It has meanwhile been successfully tested in one-dimensional model systems [41,42] and will be developed further. Recently, RTA has been successfully implemented as dissipative extension of TDLDA for finite systems and applied to the realistic test case of Na clusters [26]. This now provides an affordable and efficient approach to dissipation in finite fermion systems.

The present paper uses RTA to study systematically the dynamics of Na clusters during and after laser excitation in dependence on the key laser parameters, frequency, intensity, and pulse length. At the side of observables, we concentrate here on the energy balance. To this end we introduce the various contributions to the excitation energy, namely intrinsic kinetic and potential energy, charging energy, and energy loss by electron emission. The paper is organized as follows. In Section 2, we summarize the numerical handling of TDLDA and the RTA scheme. In Section 3, we introduce the key observables used in this study, namely the various contributions to the energy. In Section 4, we present the results, especially the energy balance as function of the various laser parameters. Further technical details are provided in appendices.

2 Formal framework

2.1 Implementation of TDDFT

Basis of the description is mean-field dynamics with Time-Dependent Density Functional Theory (TDDFT). Actually, we employ it at the level of the Time-Dependent Local-Density Approximation (TDLDA) treated in the real time domain [1,2]. It is augmented by a Self-Interaction Correction (SIC) approximated by average-density SIC (ADSIC) [43] in order have correct ionization potentials [44], which is crucial to simulate electron emission properly. The time-dependent Kohn-Sham equations for mean field and single-electron wave functions are solved with standard techniques [45,46]. The numerical implementation of TDLDA is done in standard manner [45,46]. The coupling to the ions is explicit and mediated by soft local pseudopotentials [47]. The electronic exchange-correlation energy functional is taken from Perdew and Wang [48].

The Kohn-Sham potential is handled in the Cylindrically Averaged Pseudo-potential Scheme (CAPS) [49,50], which has proven to be an efficient and reliable approximation for metal clusters close to axial symmetry. Wavefunctions and fields are thus represented on a 2D cylindrical grid in coordinate space [51]. For the typical example of the Na_{40} cluster, the numerical box extends up to 104 a_0 in radial direction and 208 a_0 along the z-axis, while the grid spacing is 0.8 a_0. We use a large set of s.p. states to supply sufficient space for thermalization. It reaches to 2.7 eV above the chemical potential covering 2∗84 spin-degenerated s.p. states with maximal azimuthal angular momentum $l_z = 6\hbar$. To solve the (time-dependent) Kohn-Sham equations for the single particle (s.p.) wavefunctions, we use time-splitting for time propagation [52] and accelerated gradient iterations for the stationary solution [53]. The Coulomb field is computed with successive over-relaxation [51]. We use absorbing boundary conditions [45,54], which gently absorb all outgoing electron flow reaching the boundaries of the grid. The difference between the initial number of electrons and the actual number of electrons left in the simulation box is thus a measure for ionization in terms of $N_{\rm esc}$, the number of escaped electrons.

The external laser field is described as a classical electro-magnetic wave in the long wavelengths limit. This augments the Kohn-Sham Hamiltonian by a time-dependent external dipole field

$$U_{\rm ext}(\mathbf{r},t) = e^2\mathbf{r}\cdot\mathbf{e}_z\, E_0\, \sin(\omega_{\rm las}t) f(t), \tag{1}$$

$$f(t) = \sin^2\left(\pi\frac{t}{T_{\rm pulse}}\right)\theta(t)\theta(T_{\rm pulse}-t). \tag{2}$$

The laser features therein are: the (linear) polarization $\mathbf{e}_z$ along the symmetry axis, the peak field strength E_0 related to laser intensity as $I_0 \propto E_0^2$, the photon frequency $\omega_{\rm las}$, and the total pulse length $T_{\rm pulse}$. The latter is related to the full width at half maximum (of intensity) as FWHM $\simeq T_{\rm pulse}/3$.

The basic building block, namely mean-field propagation of the s.p. wavefunctions $\phi_\alpha(t)$ according to TDLDA, can be summarized formally as

$$|\phi_\alpha(t)\rangle = \hat{U}(t,t')|\phi_\alpha(t')\rangle, \tag{3a}$$

$$\hat{U}(t,t') = \hat{\mathcal{T}}\exp\left(-\mathrm{i}\int_t^{t'}\hat{h}(t'')dt''\right), \tag{3b}$$

$$\hat{h}(t) = \frac{\hat{p}^2}{2m} + U_{\rm KS}[\rho(\mathbf{r},t)], \tag{3c}$$

where $\hat{U}(t,t')$ is the unitary one-body time-evolution operator with $\hat{\mathcal{T}}$ therein being the time-ordering operator, $\hat{h}$ is the Kohn-Sham mean-field operator, and $U_{\rm KS}$ is the (density dependent) actual Kohn-Sham potential [55].

2.2 Brief review on RTA

Mere TDLDA is formulated in terms of a set of occupied single-particle (s.p.) wavefunctions $\{|\phi_\alpha(t)\rangle, \alpha = 1,\ldots,N\}$ propagating according to equation (3). So far, TDLDA deals with pure Slater states. Dissipation leads inevitably to mixed states. These can be described compactly by the one-body density operator, which reads, in natural orbitals representation,

$$\hat{\rho} = \sum_{\alpha=1}^{\Omega} |\phi_\alpha\rangle W_\alpha \langle\phi_\alpha| \tag{4}$$

where Ω is the size of the configuration space, which is significantly larger than the actual electron number N. The weight W_α represents the occupation probability for s.p. state $|\phi_\alpha\rangle$. The pure mean-field propagation leaves the occupation weights W_α unchanged and propagates only the s.p. states, such that $\hat{\rho}(t) = \sum_{\alpha=1}^{\Omega} |\phi_\alpha(t)\rangle W_\alpha \langle\phi_\alpha(t)| = \hat{U}(t,0)\hat{\rho}(0)\hat{U}^{-1}(t,0)$ with $\hat{U}$ according to equation (3b).

Dynamical correlations generate changes also for the occupation weights. The RTA describes this in terms of the density-matrix equation [26]

$$\partial_t\hat{\rho} + \mathrm{i}\big[\hat{h}[\varrho], \hat{\rho}\big] = \frac{1}{\tau_{\mathrm{relax}}}\left(\hat{\rho} - \hat{\rho}_{\mathrm{eq}}[\varrho, \mathbf{j}, E]\right), \tag{5a}$$

where $\hat{h}[\varrho]$ is the Kohn-Sham Hamiltonian equation (3c) in LDA (with ADSIC) depending on the actual local density distribution $\varrho(\mathbf{r},t) = \sum_\alpha W_\alpha |\phi_\alpha(\mathbf{r},t)|^2$. The right-hand-side stands for the collision term in RTA. It describes relaxation towards the local-instantaneous equilibrium state $\hat{\rho}_{\mathrm{eq}}[\varrho, \mathbf{j}, E]$ for given local density ϱ, current distribution $\mathbf{j}$ and total energy E. The relaxation time τ_{relax} is estimated in semi-classical Fermi liquid theory. For metal clusters serving in the following as test cases, it becomes

$$\frac{\hbar}{\tau_{\mathrm{relax}}} = 0.40\frac{\sigma_{\mathrm{ee}}}{r_s^2}\frac{E^*_{\mathrm{intr}}}{N}, \tag{5b}$$

where E^*_{intr} is the intrinsic (thermal) energy of the system, N is the actual number of electrons, σ_{ee} is the in-medium electron-electron cross section, and $r_s = (3/(4\pi\overline{\varrho}))^{2/3}$ is the Wigner-Seitz radius of the electron cloud [26]. It employs an average density $\overline{\varrho}$ because τ_{relax} is a global parameter. This approximation is legitimate for metallic systems where the electron density is rather homogeneous remaining generally close to the average. Note that the in-medium cross section σ_{ee} also depends on this average density through the density dependence of screening. The actual σ_{ee} is taken from the careful evaluation of [56,57] computing electron screening for homogeneous electron matter in Thomas-Fermi approximation. This yields $\sigma_{\mathrm{ee}} = 6.5\ a_0^2$ for the case of small Na clusters whose Wigner-Seitz radius at $T = 0$ becomes typically $r_s \approx 3.7\ a_0$, somewhat smaller than the bulk value due to surface tension. These are the values which are used throughout this paper for the RTA relaxation time. This value of r_s will also be used in the jellium calculations of Section 4.5 for the sake of consistency.

The most demanding task is to determine the instantaneous equilibrium density-operator $\hat{\rho}_{\mathrm{eq}}[\varrho, \mathbf{j}, E]$ in the RTA equation (5a). It is the thermal mean-field state of minimum energy under the constraints of given local density $\varrho(\mathbf{r})$, local current $\mathbf{j}(\mathbf{r})$, and total energy E. For the wavefunctions we use the density constrained mean-field (DCMF) techniques as developed in [58], extended to account also for the constraint on current $\mathbf{j}(\mathbf{r})$. The s.p. states come along with occupations weights $W_\alpha^{(\mathrm{eq})}$ according to thermal equilibrium. The temperature T is tuned to reproduce the desired total energy E. For details of this cumbersome procedure see [26].

Once this DCMF step is under control, the RTA scheme is straightforward. The collision term in equation (5a) is evaluated at time intervals Δt, typically 0.25 fs and for high laser frequencies somewhat shorter. In between, the s.p. wavefunctions in the one-body density are propagated by mean-field evolution equation (3b). Once one time span Δt is completed, we stay at time $t + \Delta t$ and evaluate the collision term. First, the actual ϱ, $\mathbf{j}$, and E are computed. These are used to determine the local-instantaneous equilibrium state $\hat{\rho}_{\mathrm{eq}}$. This is used to step to the new one-body density $\rho(t + \Delta t) = \tilde{\rho} + (\Delta t/\tau_{\mathrm{relax}})\big(\hat{\rho} - \hat{\rho}_{\mathrm{eq}}[\varrho, \mathbf{j}, E]\big)$. In a final clean-up, this new state $\rho(t + \Delta t)$ is mapped into natural orbitals representation equation (4), thus delivering the new s.p. wavefunctions $\varphi_\alpha(t + \Delta t)$ and occupation weights $W_\alpha(t + \Delta t)$ from which on the next step is performed. For more details see again [26].

3 Energies as key observables

In our previous paper on RTA, we have concentrated on thermalization processes, in particular on relaxation times [26]. Here, we are going to employ RTA to study the energy balance in metal clusters excited by strong laser fields. The key observables are the various contributions to the energy which we will introduce in this section. The expressions assume tacitly a numerical representation of wavefunctions and fields on a spatial grid in a finite box with absorbing boundaries. In particular, the boundaries require some care as we will see.

The basic question we aim to analyze here is how the energy absorbed by the laser is "used" by the cluster and redistributed into various well identified components. The starting quantity will thus be the energy absorbed by the laser which we denote by E_{abs}. The basic energy branching channels of the cluster consist in electron emission and intrinsic heating [26]. Thus we have to analyze both these components separately. Electron emission corresponds to charge loss associated with energy loss because the emitted electrons carry some energy outwards. We denote this energy by $E_{\mathrm{ch,loss}}$. But electron emission also affects the cluster itself. It charges the cluster which is associated with a change in potential energy $E_{\mathrm{ch,pot}}$. The remaining energy delivered by the laser is shared between collective kinetic energy E_{coll} and "intrinsic" excitation energy of the electron cloud itself consisting of a kinetic $E_{\mathrm{intr,kin}}$ and a potential $E_{\mathrm{intr,pot}}$ component. All terms, of course,

sum up to $E_{\rm abs}$:

$$E_{\rm abs} = E_{\rm ch,loss} + E_{\rm ch,pot} + E_{\rm intr,kin} + E_{\rm intr,pot} + E_{\rm coll}. \quad (6)$$

Let us now specify these various contributions in more detail. This implies that we also take care of small components related to the treatment of absorbing boundaries conditions and which have to be properly accounted for in the energy balance. Moreover, we introduce as auxiliary quantity the actual total energy $E(t)$ of the system which is a crucial input for the RTA step. The various energy components are thus computed as follows:

1. $\boldsymbol{E_{\rm abs}}$ **= Energy absorbed from the laser field:**

$$E_{\rm abs} = \int_0^t dt' \int d^3r \mathbf{E}_0(t') \cdot \mathbf{j}(\mathbf{r}, t') - E_{\rm abs}^{\rm (mask)} \quad (7)$$

where $E_{\rm abs}^{\rm (mask)}$ is a correction for the particle loss at the absorbing bounds (for details see Appendix A).

2. $\boldsymbol{E(t)}$ **= total energy:**

$$E(t) = E^*_{\rm TDLDA}(t) + E_{\rm pot,bc}, \quad (8)$$

$$E_{\rm pot,bc} = \int_0^t dt' \int d^3r\, (1 - \mathcal{M}^2) U_{\rm KS} \rho(\mathbf{r}, t'). \quad (9)$$

Thereby $E^*_{\rm TDLDA}(t) = E_{\rm TDLDA}(t) - E_{\rm g.s.}$ is the energy $E_{\rm TDLDA}(t)$ computed with the given LDA + ADSIC functional taken relative to the static ground state (g.s.) energy $E_{\rm g.s.}$. The $E_{\rm pot,bc}$ is a correction for the small amount of binding energy carried in the absorbed electrons, an artifact which arises due to finite numerical boxes. Altogether, $E(t)$ accounts for the energy left within the simulation box as result of energy absorption from the laser and energy loss through ionization.

3. $\boldsymbol{E_{\rm ch,loss}}$ **= energy loss by electron emission**:

$$E_{\rm ch,loss} = E_{\rm abs} - E(t). \quad (10)$$

It represents the kinetic energy carried away by the emitted electrons.

4. $\boldsymbol{E_{\rm ch,pot}(Q)}$ **= charging energy**:

$$E_{\rm ch,pot}(Q) = E_{\rm g.s.}(Q) - E_{\rm g.s.,initial} - E_{\rm pot,bc} \quad (11)$$

where $E_{\rm g.s.}(Q)$ is the g.s. energy (i.e. temperature $T = 0$) for a given charge state Q and $E_{\rm g.s.,initial} = E(t{=}0)$ the initial ground state energy. It is augmented by the correction for lost potential energy $-E_{\rm pot,bc}$ to compensate for the corresponding term in equation (8). The $E_{\rm ch,pot}(Q)$ accounts for the excitation energy invested for charging the cluster.

5. $\boldsymbol{E_{\rm intr,kin}}$ **= intrinsic kinetic energy:**

$$E_{\rm intr,kin} = E_{\rm TDLDA}(t) - E_{\rm DCMF}(\varrho, \mathbf{j}, T{=}0) \quad (12)$$

where $E_{\rm TDLDA}(t)$ is the actual LDA + ADSIC energy and $E_{\rm DCMF}(\varrho, \mathbf{j}, T = 0)$ the DCMF energy at $T = 0$ (=ground state for fixed ϱ and $\mathbf{j}$). The computation is simplified by exploiting the fact that ϱ and $\mathbf{j}$ remain frozen in DCMF and thus also the Kohn-Sham potential. This allows to take the difference of the sums of s.p. kinetic energies between the two configurations.

6. $\boldsymbol{E_{\rm intr,pot}}$ **= intrinsic potential energy:**

$$E_{\rm intr,pot} = E_{\rm DCMF}(\rho, \mathbf{j}{=}0, T{=}0) - E_{\rm g.s.}(Q). \quad (13)$$

This is the "potential" energy stored in the constraint on given ρ & $\mathbf{j}$ at $T = 0$.

7. $\boldsymbol{E_{\rm coll}}$ **= collective flow energy:**

$$E_{\rm coll} = \int d^3r \frac{\mathbf{j}^2(\mathbf{r})}{2m\rho(\mathbf{r})}. \quad (14)$$

This is the kinetic energy which is contained in the average momentum distribution $\mathbf{j}(\mathbf{r})$. It is to be noted that $E_{\rm coll} = E_{\rm DCMF}(\rho, \mathbf{j}, T = 0) - E_{\rm DCMF}(\rho, \mathbf{j} = 0, T = 0)$. This shows that $E_{\rm coll}$ is part of the intrinsic energy.

For the balance plots below, we consider also the relative contributions $E_{\rm ch,loss}/E_{\rm abs}$, $E_{\rm ch,pot}/E_{\rm abs}$, $E_{\rm intr,kin}/E_{\rm abs}$, $E_{\rm intr,pot}/E_{\rm abs}$, and $E_{\rm coll}/E_{\rm abs}$ adding up to one. Moreover, we use the completeness equation (6) to deduce $E_{\rm intr,pot}$ from the other energies. This saves another costly DCMF evaluation for $E_{\rm DCMF}(\varrho, \mathbf{j} = 0, T = 0)$ in the definition equation (13).

It is to be noted that the evaluation of the intrinsic kinetic energy equation (12) had been used in the past often with a semi-classical estimate [45], for details see Appendix B. This is much simpler to evaluate, but not precise enough for the present purposes. We must use here the more involved, exact definition. Fortunately, this is no problem in connection with RTA because we compute the expensive DCMF state anyway and so get the correct quantum mechanical value equation (12) for free.

Besides energies, we will occasionally look also at two other observables, the average ionization as number of electrons escaped from the numerical box $N_{\rm esc}$ and the dipole momentum $\mathbf{D}$, defined as

$$N_{\rm esc}(t) = N(t{=}0) - \int d^3r\, \rho(\mathbf{r}, t), \quad (15)$$

$$\mathbf{D}(t) = \int d^3r\, \mathbf{r}\rho(\mathbf{r}, t). \quad (16)$$

It is important for all observables to keep in mind that TDLDA produces averages. For example, $N_{\rm esc}$ represents the ionization averaged over an ensemble of similar processes; a detailed distribution of (integer) ionization stages can be recovered approximately from the final wavefunctions [59]. This last step of analysis, namely unfolding distributions of energies and ionization, will not be considered here.

4 Results and discussion

In the previous RTA paper [26], we had briefly looked at dissipation effects as function of laser frequency for constant intensity and found that dissipation is strong if the laser is in resonance with a system mode and weak otherwise. This is a trivial result in view of equation (5b): the relaxation rate increases with excitation energy and

excitation energy is large at resonance. In order to eliminate this trivial trend, we consider here variation of laser parameters for fixed absorbed energy $E_{\rm abs}$ tuning the intensity such that the wanted value for $E_{\rm abs}$ is maintained. We calibrate the laser parameters this way for the case of pure TDLDA and use the same parameters then also for RTA. The resulting $E_{\rm abs}$ is in most situations the same. A difference in $E_{\rm abs}$ between RTA and TDLDA, if it occurs, is then already a message.

One of the interesting topics related to energy balance is the question of appearance size, the limit of fission/fragmentation stability of a metal cluster for a given charge state [23,24]. It is the lower the more gentle one can arrange ionization. The systematics of energy balance will tell us how to ionize most gently or, in reverse, to heat most efficiently. The purpose of this paper is to analyze how relaxation processes do affect energy balance in laser or collisional irradiation processes. For this we use the energy observables discussed in Section 3. This various energies are not directly measurable in experiments. A direct comparison between the present computations and experimental results would require additional measures (e.g., photo electron spectra, time resolved observation, coincidence cross sections). This goes beyond the scope of the present paper. Still, the effects observed in our results can serve for qualitative interpretation of some experimental observables, such as ionization, extensively discussed in this paper. In the following discussion of our results we shall thus remain at this level of analysis with only qualitative links to experiments.

4.1 Typical time evolution of energies

The lower panel of Figure 1 shows the time evolution of the five contributions equation (6) to the energy stacked in a balance manner. Each colored band represents the contribution indicated in the key to the right side of the panels. Upper and middle panels show as complementing information dipole moment and ionization. The case $\omega = 2.7$ eV shown in Figure 1 corresponds to a resonant excitation at the Mie plasmon frequency. We see this from the time evolution of ionization $N_{\rm esc} \equiv Q$ and dipole. The TDLDA result (right panels) shows ongoing dipole oscillations and, connected with that, ionization carries on long after the laser pulse has terminated. However, the RTA ionization (upper left panel) turns gently to a constant $N_{\rm esc}$. This is achieved by the dissipation in RTA which damps the dipole signal. This highly resonant case reveals a marked qualitative difference between TDLDA and RTA. We thus see that long-time TDLDA simulations have to be taken with care because they overestimate the long-lasting reverberations of the dipole. This point is conceptually very important. The above mentioned defect of TDLDA is generic. It arises particularly if the dynamics couples to a resonant state and is related to the fact that this coupling is not properly damped in TDLDA thus leading to spurious long term oscillations with subsequent long lasting emission. This makes the analysis of final states of a system questionable, especially in sufficiently massive clusters with high spectral density for which resonant coupling is abundant. The interesting aspect here is that RTA precisely cuts this effect by damping the long lasting dipole oscillations and so allows a better founded analysis of final states.

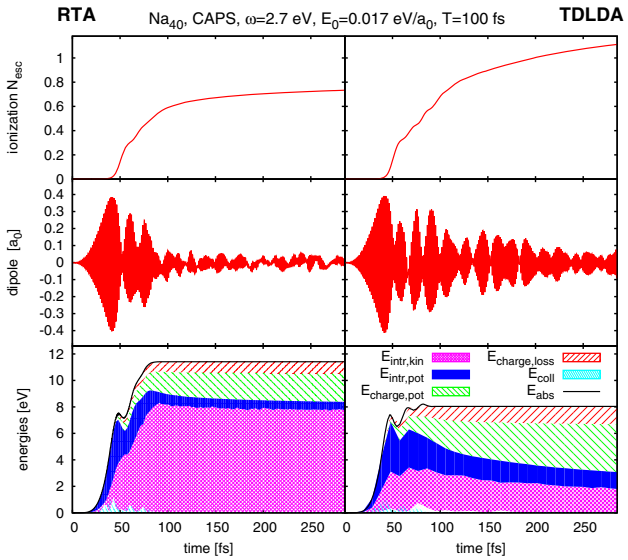

Fig. 1. Time evolution of ionization (upper panels), dipole moment (middle panels), and energies (lower panels) for the case of Na_{40} in CAPS excited by a laser with frequency $\omega = 2.7$ eV, total pulse length $T_{\rm pulse} = 100$ fs, and intensity $I = 1.3 \times 10^{10}$ W/cm^2. Left panels show results from RTA and right panels from TDLDA. The lower panels show the total absorbed energy (black line) ad the four different contributions stacked one above the other.

The difference in ionization also shows up as a difference in energy consumption by ionization (areas $E_{\rm charge,loss}$ plus $E_{\rm charge,pot}$) such that eventually TDLDA produces relatively less intrinsic excitation energy in than RTA.

The lower panels of Figure 1 also show the collective kinetic energy equation (14). It plays a role in the initial stages of excitation. The reason is that the dipole field of the laser couples to the collective dipole operator thus depositing its energy first in collective dipole flow. However, the large spectral fragmentation of the dipole mode (Landau damping) [60,61] spreads the collective energy very quickly over the dipole spectrum. The large fragmentation width of the actual test case Na_{40} produces a relaxation time of about 2 fs for this Landau damping and this relaxation is active already at mean field level. As a consequence, collective kinetic energy never grows large for pulses much longer 2 fs and becomes negligible soon after the laser pulse is extinguished. We will ignore it in the following analysis evaluated at late stages of cluster dynamics.

It is remarkable that RTA allows to absorb much more energy $E_{\rm abs}$ from the laser, although exactly the same pulse is used in both cases. This is a particular feature of resonant excitation related to Rabi oscillations [62]. The external field quickly induces dipole

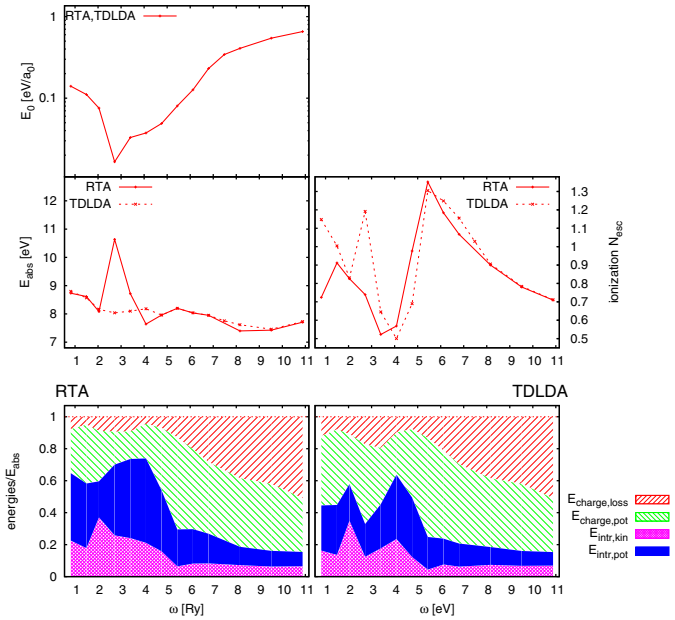

Fig. 2. Various observables from RTA (full lines) and TDLDA (dashed lines) evaluated at final time of the simulations at 300 fs. Pulse length was $T_{\rm pulse} = 100$ fs throughout. Intensity has been tuned such that $E_{\rm abs} \approx 8.2$ eV for TDLDA. Upper left: field strength E_0 ($\propto\sqrt{I}$). Middle left: total absorbed energy $E_{\rm abs}$. Middle right: ionization $N_{\rm esc}$. Lower: balance of relative energies (energy contributions divided by total absorbed energy $E_{\rm abs}$). Left panel for RTA and right one for TDLDA.

oscillations of the electron cloud. This dipole excitation, once sufficiently large, leads to stimulated emission and so reduces excitation. This can be seen from oscillations of $E_{\rm abs}$ where phases of energy absorption are interrupted by phases of energy loss back to the laser field. Now in RTA, dissipation serves as a competing de-excitation channel which reduces stimulated emission and so paves the way to more stimulated absorption. This mechanism is less important off resonance where we observe generally less differences between RTA and TDLDA as we will see in the upper panel of Figure 2.

4.2 Trends with laser frequency

The main intention of the study is to figure out trends with laser parameters. To this end, we simulate each case for a time of 300 fs and collect the results at this final time. This is a safe procedure for the majority of non-resonant cases. It is incomplete for resonant excitation, at least with TDLDA. In the latter case, we have to keep in mind that the contribution of emission is somewhat underestimated and that of intrinsic energy overestimated. The major trends remain, nonetheless, the same.

Figure 2 shows the energy contributions and other observables as function of laser frequency ω. The laser intensity is tuned for each frequency such that the absorbed energy is about the same, namely $E_{\rm abs} \approx 8.2$ eV, for TDLDA. The same field strength is then used also for RTA and the emerging $E_{\rm abs}$ may then be different. This is indeed seen in the left middle panel where just near the Mie plasmon resonance (≈2.7 eV) RTA absorbs much more energy, as was discussed already in connection with Figure 1.

The upper left panel of Figure 2 shows the field strength E_0. The Mie plasmon resonance is visible as marked dip at $\omega = 2.7$ eV because resonance means that more response is achieved with less impact. The steady growth of E_0 for larger frequencies complies with the Keldysh formula where the effective field strength shrinks $\propto\omega^{-2}$ [63].

The middle right panel shows ionization $N_{\rm esc}$. At lower frequencies, RTA suppresses emission significantly. Obviously, more of the absorbed energy is turned to intrinsic excitation (thermalization). Quite different is the behavior at high frequencies above ionization potential (IP) in which case TDLDA and RTA deliver almost the same ionization.

The lower panels disentangle the absorbed energy into its four relevant contributions (6). Again, we see that TDLDA and RTA differ most at the side of lower energies, particularly near the Mie plasmon resonance. There is practically no difference from $\omega \approx 6.1$ eV on. This $\omega = 6.1$ eV is a very prominent point. It is just the frequency from which on all occupied valence electrons of Na_{40} can be emitted by a one-photon process. The IP at 3.5 eV sets the frequency where the HOMO can be removed by one photon. The region 3.5–6.1 eV covers the transition from the onset of one-photon processes for the least bound state to an "all inclusive" one-photon ionization. And we see, indeed, how TDLDA and RTA results come stepwise closer to each other in this region.

The lower panels of Figure 2 show the results in form of energy balance where the filled areas visualize a given contribution, as indicated. Areas $E_{\rm charge,loss}$ and $E_{\rm charge,pot}$ together show the amount of energy spent for ionization while areas $E_{\rm intr,kin}$ and $E_{\rm intr,pot}$ together illustrate the part of intrinsic energy. The balance plot makes the trends of intrinsic energy immediately visible. Its fraction is largest around resonance and smallest above the point of "all one photon" ionization near $\omega = 6.1$ eV. This trend holds for RTA as well as for TDLDA. What differs are the actual fractions of intrinsic energy, generally being somewhat larger for RTA. But the fractions are not so dramatically different as one may have expected from the plot of energies as such in Figure 1. Division by $E_{\rm abs}$ and the often larger $E_{\rm abs}$ in RTA reduces the effect for the fractions of energy.

Already at this point, we can give a first answer to the question of how to ionize most gently or to heat most efficiently. Least intrinsic energy relative to most electron output is achieved near the point from which on all electrons can be removed by one photon which is 6.1 eV in the present case. Most heating is obtained below, particularly near resonance or for very low frequencies.

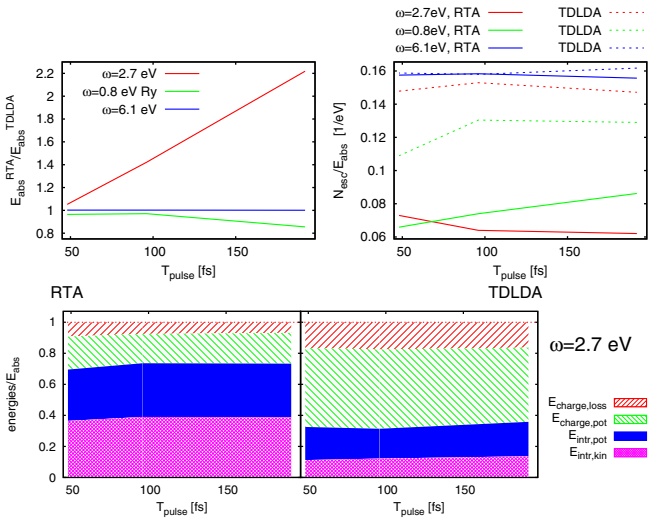

Fig. 3. Lower panel: energy balance as function of pulse length $T_{\rm pulse}$ for Na_{40} excited by a laser with frequency $\omega = 2.7$ eV and intensity tuned to $E_{\rm abs}^{\rm (TDLDA)} \approx 8.2$ eV. Left upper panel: The ratio $E_{\rm abs}^{\rm (RTA)}/E_{\rm abs}^{\rm (TDLDA)}$ for three different frequencies as indicated, resonant $\omega = 2.7$ eV and off-resonant $\omega = 0.8, 6.1$ eV. Right upper panel: ratio $N_{\rm esc}/E_{\rm abs}$ of emitted electrons per absorbed energy for the three frequencies as in the left panel and separately for RTA (full lines) as well as TDLDA (dashed lines).

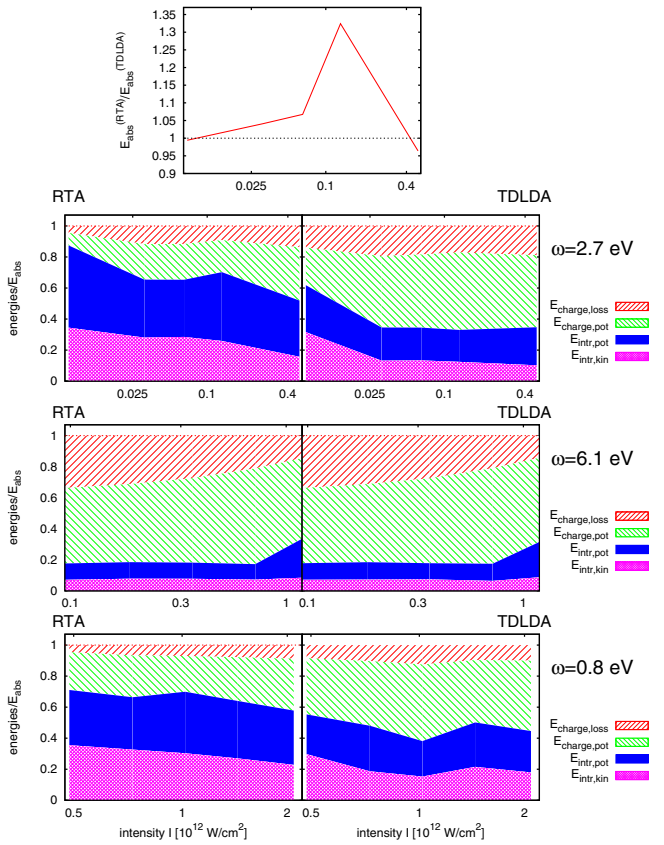

Fig. 4. Lower three panels: energy balance as function of laser intensity I for Na_{40} excited by a laser with three different frequencies as indicated and pulse length $T_{\rm pulse} = 100$ fs. Upper panel: ratio of absorbed energy between RTA and TDLDA for the resonant case ($\omega_{\rm las} = 2.7$ eV) also as function of laser intensity I.

4.3 Trends with pulse length $T_{\rm pulse}$

Figure 3 shows the effect of laser pulse length $T_{\rm pulse}$. The lower panels show the energy balance. as function of $T_{\rm pulse}$ for the resonant case $\omega = 2.7$ eV. The trends with $T_{\rm pulse}$ are extremely weak, even for the most sensitive case of resonant excitation. They are equally weak for other frequencies. Thus these are not shown.

One interesting aspect pops up, again, concerning the amount of absorbed energy. This is illustrated in the upper panel of Figure 3 showing the ratio from RTA to TDLDA, $E_{\rm abs}^{\rm (RTA)}/E_{\rm abs}^{\rm (TDLDA)}$, for three frequencies standing for the three typical regions, very low frequency (0.8 eV), resonance (2.7 eV), and above threshold for direct ionization of all shells (6.1 eV). The energy ratio increases dramatically with pulse length in the resonant case $\omega = 2.7$ eV. Although the partition of energies changes very little, the total output becomes much larger with RTA for long pulses. This happens because dissipation steadily removes energy from the coherent dipole oscillations thus keeping the door open for ongoing energy absorption while in TDLDA energy loss by stimulated emission limits energy take-up, see the discussion in Section 4.1. For off-resonant cases, the ratio $E_{\rm abs}^{\rm (RTA)}/E_{\rm abs}^{\rm (TDLDA)}$ stays close to one as can be seen here for low frequency $\omega = 0.8$ eV and for high frequency 6.1 eV.

4.4 Trends with laser intensity

The three lower panels of Figure 4 show the effect of laser intensity I (or field strength E_0, respectively) for three frequencies, low $\omega = 0.8$ eV, resonant $\omega = 2.7$ eV, and high $\omega = 6.1$ eV which is on the onset of the one-photon regime for all occupied s.p. states. For the low frequency case and at resonance, intrinsic energy shrinks with increasing I. The reason is that higher order photon processes become increasingly important which, in turn, enhances the contribution from direct (multi-photon) emission leaving less energy to dissipate. For resonant excitation, we have the additional effect that the Mie plasmon frequency is increasing with increasing I because ionization is stronger and enhances the charge state of the cluster [60]. Thus the resonance frequency is running away from the laser frequency which also reduces dissipation. For the high-frequency case $\omega = 6.1$ eV, the intrinsic energy increases with I. This is, again, an effect of ionization which drives the IP up and thus moves large parts of the s.p. states out of the one-photon regime back to the multi-photon regime. Differences between the frequencies shrink with increasing I because the fraction of intrinsic energy decreases with I for the low and medium frequencies thus approaching the high frequency case (related to direct emission). This is better visible within the given span of I for RTA while it requires even larger I to be seen for TDLDA. The effect is plausible because large I means that we come into

the field dominated regime where frequencies become less important and where direct field emission takes over [64].

The upper panel of Figure 4 shows the ratio of absorbed energy $E_{\rm abs}^{\rm (RTA)}/E_{\rm abs}^{\rm (TDLDA)}$ as function of field strength for the resonant frequency $\omega_{\rm las} = 2.7$ eV. This case, unlike the non-resonant frequencies, shows a peak at a certain field strength. This emerges as combination from several features seen before. At small intensities, there is little energy deposited, thus little dissipation and RTA does not differ much from TDLDA. More energy becomes absorbed with increasing intensity which is converted preferably to intrinsic energy in the resonant case opening subsequently the pathway to more absorption. This explains the increase from low I on upwards. For larger amounts of absorbed energy, the enhanced dissipation broadens the resonance thus reducing resonant response at peak frequency. This explains the decrease of the ratio for further increasing intensities.

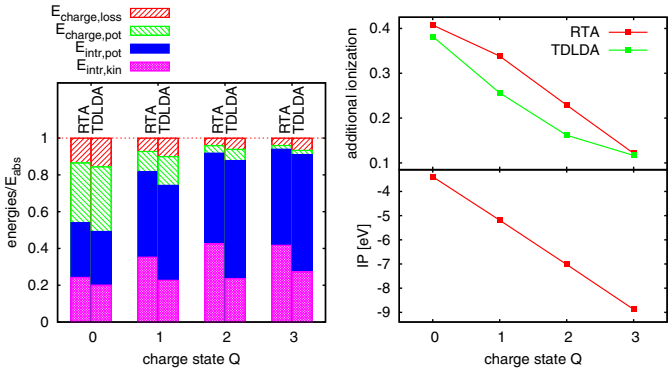

Fig. 5. Results for clusters Na_{40+Q}^{+Q} which have $N_{\rm el} = 40$ electrons and varied charges state Q. The ionic structure is approximated by soft spherical jellium model with Wigner-Seitz radius $r_s = 3.65\ a_0$ and surface parameters $\sigma = 1\ a_0$ [45,65]. All clusters are excited initially by an instantaneous boost with boost energy $E_{\rm abs} = 2.7$ eV. Left panel: energy balance for Na, plotting RTA and TDLDA side by side. Lower right: ionization potential (IP). Upper right: ionization induced by boost.

4.5 Impact of cluster charge

For the one reference system Na_{40}, we have so far studied laser excitation with extensive exploration of the rich variety of laser parameters. We are now going to vary the systems under consideration, studying clusters of the form Na_{40+Q}^{+Q} which have $N_{\rm el} = 40$ electrons and varied initial charge state Q. It would not make sense to scan all laser parameters for each system anew. Thus we take as a means of comparison an instantaneous dipole boost $\varphi_\alpha \to \exp(-{\rm i}\, p_0\, z)\varphi_\alpha$ applied to all s.p. wavefunctions in the same manner [45,46]. The boost momentum p_0 regulates its strength associated with the initial excitation energy $E_{\rm abs} = Np_0^2/(2m)$ which can be compared with the absorbed energy in the laser case. The boost excitation touches all modes of a system at once with some bias on resonant excitation and it has only one parameter which simplifies global comparisons between different systems. We will thus use boost excitation in this section for variation of cluster charge and in the next section for cluster size.

There is another subtle problem when varying cluster charge: the ionic geometry changes with charge state. This can become particularly pronounced for deformed clusters. Thus we consider variation of charge for a magic electron number, actually $N_{\rm el} = 40$. This forces all systems for any charge state to near spherical geometry. In this particular section we thus go one step further and exclude any geometry effect by using a soft jellium density for the ionic background [45,65]. The result for charge balance after boost excitation with initial energy of 2.7 eV is shown in Figure 5. We see again the typical pattern: about equal share of intrinsic kinetic and intrinsic potential, about factor 2 more energy invested charging the cluster than energy lost by emission, and somewhat more intrinsic energy in RTA as compared to TDLDA. The new feature here is that we see a strong trend of the intrinsic energy versus energy loss by emission. Electron emission decreases with increasing charge state Q because the IP increases with Q which enhances the cost of emission. In turn, less energy is exported by emission and invested into charging energy while more energy is remaining in the clusters for dissipation into intrinsic excitation energy. The trend is clear, simple, and monotonous. It will apply equally well in other systems (with varying IP) and other observations. For example, laser frequency scans for different charge states will show the same pattern as function of frequency, but with an increasing offset of intrinsic energy with increasing charge state.

4.6 Impact of cluster size

We have also compared RTA with TDLDA for clusters of different size considering a series of closed-shell systems Na_9^+, Na_{21}^+, Na_{41}^+, as well as open-shell systems Na_{15}^+, Na_{33}^+. This sample allows to explore trends with system size as well as the effect of shell closures. As for variation of charge in the previous section, we avoid a tedious scan of frequencies and other laser parameters by using simply a boost excitation. Two boost strengths are considered, $E_{\rm boost}/N_{\rm el} = 0.027$ eV still in the linear regime and a higher $E_{\rm boost}/N_{\rm el} = 0.14$ eV. Note that these boost strength are scaled to system size. This should provide comparable thermodynamic conditions (e.g. temperatures).

No clear trend with system size could be found. However, at lower excitation energies, we see a shell effect to the extend that magic systems gather more thermal energy. This shell effect is going away for the higher excitations. It is to be noted that the lower excitation strength $E_{\rm boost}/N_{\rm el} = 0.027$ eV leads in all five system to a temperature around $T = 1500$ K while the higher excitation $E_{\rm boost}/N_{\rm el} = 0.14$ eV is associated with temperature about $T = 3000$ K. This matches with observations from shell structure in medium sized Na clusters where shell effects become negligible at about $T = 2000$ K (we deduce this from the fact that the shell correction energy drops

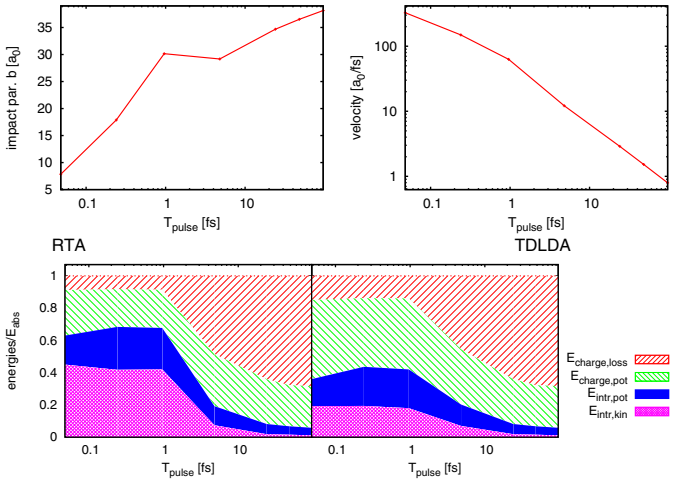

Fig. 6. Lower panel: energy balance as function of pulse length $T_{\rm pulse}$ for Na_{40} excited through a bypassing ion. The impact parameter b is tuned to provide $E_{\rm abs}^{\rm (TDLDA)} \approx 8.1$ eV. Upper panel: pulse length $T_{\rm pulse}$ and excitation strength can be translated to an impact parameter b (upper left) and ion velocity v (upper right). This is done here for an Ar ion with charge $Q = 8$.

$\propto T \exp\left(-\frac{20}{\hbar\omega}T\right)$ with $\hbar\omega = 3.4\ \text{eV}/N^{1/3}$ [66] and assume the dividing line at a reduction by factor 10). The lower excitation strength here is below this critical point and the higher excitation above.

4.7 Excitation with by-passing ions

An alternative excitation mechanism is collision through a by-passing ion see, e.g., [23,25]. We simulate that by a single dipole pulse equation (1) with frequency $\omega = 0$. The result is shown in the lower panel of Figure 6. There are clearly two very different regimes. For $T_{\rm pulse} \leq 1$ fs, we encounter practically an instantaneous excitation by a Dirac δ pulse, just a boost. Here, the relations between ionization and intrinsic energy are similar to laser excitation in the multi-photon regime (frequencies below IP), see Figure 2. Much different looks the regime of very slow ions (large $T_{\rm pulse}$). The intrinsic excitation shrinks dramatically. Almost all energy flows into ionization. The efficiency of ionization is here even better than for the one-photon regime (high frequencies) in Figure 2. Thus we can conclude that collision by very slow, highly charged ions is the softest way of ionization.

The field exerted by a highly charged ion was simulated for simplicity by a single, zero frequency pulse. This can be translated into collision parameters. We have done that for an Ar ion with charge $Q = 8$ as example. The peak field strength E_0 is related to the impact parameters b as $E_0 = 8Q/b^2$ and the passing time is identified as the FWHM of field strength in the pulse which yields an estimate for the velocity as $v = 2b/T_{\rm pulse}$. The result of this identification for fixed excitation energy $E_{\rm abs} = 8.1$ eV is shown in the upper panel of Figure 6. The sample of $T_{\rm pulse}$ produces a huge span of collisional conditions.

A word is in order about the "ideal case" of slow collisions. It may be not as ideal as it looks at first glance. Mind that the impact parameter b cannot be controlled in a collision. We encounter always a mix of impact parameters thus leaving an ensemble of clusters in very different excitation stages. Slow collisions as a means to produce smaller appearance sizes work only if one can suppress sufficiently well the contributions from the more energetic reactions at low impact parameter. Laser excitation can be better controlled and we found that laser frequencies just above the ionization threshold for the whole valence shell leave also little intrinsic excitation. For a fair final comparison one has yet to produce the whole excitation cross sections, integrated over all impact parameters a task which goes beyond the scope of this paper.

5 Conclusion

In this paper, we have investigated from a theoretical perspective the effect of dissipation on the energy balance in metal clusters under the influence of strong electro-magnetic pulses. Particular attention was paid to the branching between thermalization (intrinsic energy) and ionization (charging energy, energy export by electron emission). Basis of the description was time-dependent density functional theory at the level of the Time-Dependent Local-Density Approximation (TDLDA) augmented by an averaged self-interaction correction. For a pertinent description of dissipation, we include also dynamical correlations using the Relaxation-Time Approximation (RTA). Test cases are Na clusters, mainly Na_{40} complemented by a few cases with different size and charge state.

We have investigated laser excitation looking at the dependence of energy balance on the main laser parameters, frequency, intensity (field strength), and pulse length. Frequency is found to be the most critical parameter. Dissipation is much more important for resonant excitation than for non-resonant cases. It takes away energy from the coherent dipole oscillations induced from the laser field and converts it to intrinsic energy. This, in turn, reduces the energy loss by induced photon emission and so enhances significantly the energy absorption from the laser field. The effect continues steadily and thus grows huge the longer the laser pulse. Another crucial mark is set by the ionization threshold. For frequencies below, the fraction of intrinsic excitation is generally larger than for frequencies above. Direct emission (one-photon processes) is fast and leaves dissipation no chance. Thus dissipative effects are negligible for high frequencies and RTA behaves almost identical with TDLDA. The other two laser parameters, intensity and pulse length show much less dramatic trends in the energy balance. Noteworthy are here two effects. First, the dissipative enhancement of energy absorption in the resonant case increases linearly with pulse length. Second, with increasing intensity (field strength), the transition from the frequency dominated to the field dominated regime renders the energy balance more similar for the different frequencies (i.e. independent of frequency). Field

emission in the strong field regime comes along with producing less intrinsic energy.

The impact of system charge and system size was investigated for simplicity with an instantaneous dipole boost excitation. The charge state of a cluster changes systematically the relation between electron emission and intrinsic heating in an obvious manner: the higher the charge, the harder it becomes to emit an electron and thus a larger fraction of the absorbed energy is kept in the cluster and converted to intrinsic energy. Effects of cluster size are weak. Shell structure still plays a role for small excitations and becomes unimportant for higher energies.

We have also investigated excitation by a highly charged ion passing by the cluster. There is a dramatic change of energy balance with impact parameter. Close collisions exert a short pulse which leads to significant intrinsic energy (more than 50%) if dissipation is accounted for. Distant collisions soak off electrons very gently and achieve high ionization while depositing very little intrinsic energy.

The trends of the energy balance with pulse profile and pulse parameters are all plausible. It is interesting to check these effects for other systems (bonding types, geometries). Research in this direction is underway.

This work was supported by the CNRS and the Midi-Pyrénées region (doctoral allocation number 13050239), and the Institut Universitaire de France. It was granted access to the HPC resources of IDRIS under the allocation 2014-095115 made by GENCI (Grand Equipement National de Calcul Intensif), of CalMiP (Calcul en Midi-Pyrénées) under the allocation P1238, and to the Regionales Rechenzentrum Erlangen (RRZE) of the Friedrich-Alexander university Erlangen/Nürnberg.

Author contribution statement

All three authors have contributed equally to the work being published.

Appendix A: Boundary correction to laser energy

Starting point for the computation of the energy absorbed from an external laser field is the definition in terms of the current $\mathbf{j}$ which reads

$$E^{(\mathrm{j})}_{\mathrm{abs}}(t) = \int_0^t dt' \int d^3r\, \mathbf{E}_0(t') \cdot \mathbf{j}(\mathbf{r}, t'). \tag{A.1}$$

This is turned, by virtue of the continuity equation $\partial_t \rho = \nabla \cdot \mathbf{j}$, into an expression in terms of $\partial_t \rho$, namely:

$$E^{(\rho)}_{\mathrm{abs}}(t) = \int_0^t dt' \int d^3r\, \mathbf{E}_0(t') \cdot \mathbf{r}\, \partial_t \rho(\mathbf{r}, t'). \tag{A.2}$$

This form is easier to evaluate because ρ is readily available while $\mathbf{j}$ needs to be computed separately. The problem is that the continuity equation holds only for Hermitean propagation of the s.p. wavefunctions. To be more specific, we have to write

$$\partial_t \rho_{\mathrm{herm}} = \nabla \cdot \mathbf{j} \tag{A.3}$$

where $\partial_t \rho_{\mathrm{herm}}$ is the part stemming from Hermitean propagation $\partial_t \psi_\alpha = \left[\hat{h}, \psi_\alpha\right]$. Absorbing boundaries introduce a non-Hermitean contribution to time evolution and so spoil the continuity equation for the total density. Subsequently, the relation $E^{(\mathrm{j})}_{\mathrm{abs}} = E^{(\rho)}_{\mathrm{abs}}$ is not guaranteed any more. But we can split the time-derivative of total density $\partial_t \rho$ into Hermitean part and contribution from absorbing bounds as

$$\partial_t \rho_{\mathrm{herm}} = \partial_t \rho - \partial_t \rho_{\mathrm{mask}}, \tag{A.4}$$

$$\partial_t \rho_{\mathrm{mask}} = \tfrac{1-\mathcal{M}^2}{\delta t} \textstyle\sum_\alpha |\psi_\alpha|^2 \tag{A.5}$$

where $\mathcal{M}$ is the mask function and δt is the size of the time step. This separation equation (A.4) allows to repair the relation $E^{(\mathrm{j})}_{\mathrm{abs}}$ and $E^{(\rho)}_{\mathrm{abs}}$ as

$$E^{(\mathrm{j})}_{\mathrm{abs}}(t) = E^{(\rho)}_{\mathrm{abs}} - E^{(\mathrm{mask})}_{\mathrm{abs}} \tag{A.6}$$

$$E^{(\mathrm{mask})}_{\mathrm{abs}} = \int_0^t dt'\, \mathbf{E}_0(t') \cdot \mathbf{r}\, \partial_t \rho_{\mathrm{mask}}(\mathbf{r}, t'). \tag{A.7}$$

Appendix B: On the semi-classical intrinsic energy

The fully quantum-mechanical definition equation (12) of an intrinsic kinetic energy employs a DCMF iteration which is naturally available when propagating with RTA but becomes a rather expensive extra step in pure TDLDA. Thus one often sidesteps to a simpler semi-classical estimate from the extended Thomas-Fermi approach [67]

$$E^{(\mathrm{ETF})}_{\mathrm{intr,kin}} = E^{(\mathrm{TDLDA})}_{\mathrm{kin}} - \int d^3r \left(\tfrac{2}{3}(3\pi^2)^{2/3} \rho^{2/3} + \frac{(\nabla\rho)^2}{18\rho} \right) - E_{\mathrm{coll}}$$

with the collective energy from equation (14). The two definitions are compared in Figure B.1. The semi-classical $E^{(\mathrm{ETF})}_{\mathrm{intr,kin}}$ is a robust order-of-magnitude estimate which works particularly well in the early phases of excitation.

The case is more involved than it appears in Figure B.1. Actually, the mismatch starts at $t = 0$. But we shift the value of $E^{(\mathrm{ETF})}_{\mathrm{intr,kin}}$ to match at $t = 0$, precisely because it is a semi classical estimate, thus not fully vanishing in ground state. The punishment is then a mismatch at large times. This may have to be discussed.

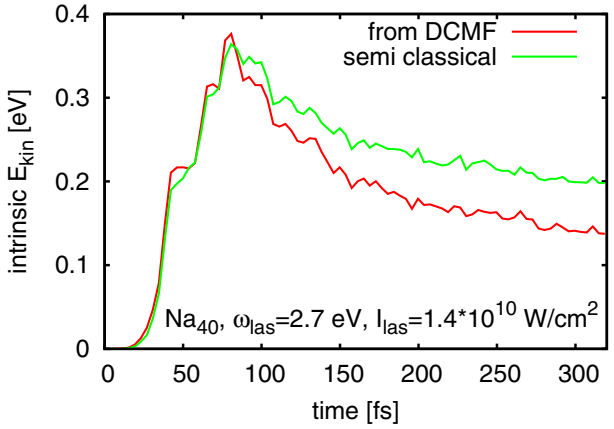

Fig. B.1. Comparison of intrinsic kinetic energy $E_{\mathrm{intr,kin}}$ from fully quantum-mechanical DCMF definition (12) with the semi-classical estimate $E^{(\mathrm{ETF})}_{\mathrm{intr,kin}}$ for the example of Na_{40} excited by a laser pulse with $\omega_{\mathrm{las}} = 2.7$ eV, $I_{\mathrm{las}} = 1.4 \times 10^{10}$ W/cm^2, and $T_{\mathrm{pulse}} = 96$ fs.

References

1. E.K.U. Gross, W. Kohn, Adv. Quant. Chem. **21**, 255 (1990)
2. E.K.U. Gross, J.F. Dobson, M. Petersilka, Top. Curr. Chem. **181**, 81 (1996)
3. M.A.L. Marques, N.T. Maitra, F.M.S. Nogueira, E.K.U. Gross, A. Rubio, *Fundamentals of Time-Dependent Density Functional Theory*, Lecture Notes in Physics (Springer-Verlag, Berlin, 2012), Vol. 837
4. J.W. Negele, Rev. Mod. Phys. **54**, 913 (1982)
5. K.T.R. Davies, K.R.S. Devi, S.E. Koonin, M.R. Strayer, in *Treatise on Heavy–Ion Physics, Compound System Phenomena*, edited by D.A. Bromley (Plenum Press, New York, 1985), Vol. 3, p. 3
6. M. Bender, P.H. Heenen, P.G. Reinhard, Rev. Mod. Phys. **75**, 121 (2003)
7. G.F. Bertsch, R. Broglia, *Oscillations in Finite Quantum Systems* (Cambridge University Press, Cambridge, 1994)
8. P.G. Reinhard, E. Suraud, in *Time-Dependent Density Functional Theory*, Lecture Notes in Physics, edited by M.A.L. Marques, C.A. Ullrich, F. Nogueira (Springer, Berlin, 2006), Vol. 706, p. 391
9. T. Fennel, K.H. Meiwes-Broer, J. Tiggesbäumker, P.G. Reinhard, P.M. Dinh, E. Suraud, Rev. Mod. Phys. **82**, 1793 (2010)
10. C. Golabek, C. Simenel, Phys. Rev. Lett. **103**, 042701 (2009)
11. V.E. Oberacker, A.S. Umar, J.A. Maruhn, P.G. Reinhard, Phys. Rev. C **82**, 034603 (2010)
12. P.G. Reinhard, C. Toepffer, Int. J. Mod. Phys. E **3**, 435 (1994)
13. G.F. Bertsch, P.F. Bortignon, R.A. Broglia, Rev. Mod. Phys. **55**, 287 (1983)
14. Y. Abe, S. Ayik, P.G. Reinhard, E. Suraud, Phys. Rep. **275**, 49 (1996)
15. V.V. Sargsyan, G.G. Adamian, N.V. Antonenko, W. Scheid, H.Q. Zhang, Phys. Rev. C **85**, 024616 (2012) [Erratum: Phys. Rev. C **85**, 069903 (2012)]
16. D. Lacroix, S. Ayik, Eur. Phys. J. A **50**, 95 (2014)
17. N.D. Fatti, R. Bouffanais, F. Valle, C. Flytzanis, Phys. Rev. Lett. **81**, 922 (1998)
18. C. Voisin, D. Christofilos, N.D. Fatti, F. Vallée, B. Prövel, E. Cottancin, J. Lermé, M. Pellarin, M. Broyer, Phys. Rev. Lett. **85**, 2200 (2000)
19. E.E.B. Campbell, K. Hansen, K. Hoffmann, G. Korn, M. Tchaplyguine, M. Wittmann, I.V. Hertel, Phys. Rev. Lett. **84**, 2128 (2000)
20. M. Schmidt, R. Kusche, T. Hippler, J. Donges, W. Kronmüller, B. von Issendorff, H. Haberland, Phys. Rev. Lett. **86**, 1191 (2001)
21. F. Fehrer, P.G. Reinhard, E. Suraud, Appl. Phys. A **82**, 145 (2006)
22. M. Kjellberg, O. Johansson, F. Jonsson, A.V. Bulgakov, C. Bordas, E.E.B. Campbell, K. Hansen, Phys. Rev. A **81**, 023202 (2010)
23. F. Chandezon, C. Guet, B.A. Huber, D. Jalabert, M. Maurel, E. Monnand, C. Ristori, J.C. Rocco, Phys. Rev. Lett. **74**, 3784 (1995)
24. U. Näher, S. Björnholm, S. Frauendorf, F. Garcias, C. Guet, Phys. Rep. **285**, 245 (1997)
25. J. Daligault, F. Chandezon, C. Guet, B.A. Huber, S. Tomita, Phys. Rev. A **66**, 033205 (2002)
26. P.G. Reinhard, E. Suraud, Ann. Phys. **354**, 183 (2015)
27. L.E. Reichl, *A Modern Course in Statistical Physics* (Wiley, New York, 1998)
28. C. Cercignani, in *The Boltzmann Equation and Its Applications*, Applied Mathematical Sciences (Springer, New York, 1988), Vol. 67
29. E.A. Uehling, G.E. Uhlenbeck, Phys. Rev. **43**, 552 (1933)
30. G.F. Bertsch, S. Das Gupta, Phys. Rep. **160**, 190 (1988)
31. D. Durand, E. Suraud, B. Tamain, *Nuclear Dynamics in the Nucleonic Regime* (Institute of Physics, London, 2000)
32. A. Domps, P.G. Reinhard, E. Suraud, Phys. Rev. Lett. **81**, 5524 (1998)
33. T. Fennel, G.F. Bertsch, K.H. Meiwes-Broer, Eur. Phys. J. D **29**, 367 (2004)
34. L.P. Kadanoff, G. Baym, *Quantum Statistical Mechanics: Green's Function Methods in Equilibrium and Nonequilibrium Problems*, Frontiers in Physics (Benjamin, New York, 1962)
35. P.L. Bhatnagar, E.P. Gross, M. Krock, Phys. Rev. **94**, 1954 (511)
36. N.W. Ashcroft, N.D. Mermin, *Solid State Physics* (Saunders College, Philadelphia, 1976)
37. D. Pines, P. Nozières, *The Theory of Quantum Liquids* (W. A. Benjamin, New York, 1966)
38. A. Dutta, C. Trefzger, K. Sengupta, Phys. Rev. B **86**, 085140 (2012)
39. P. Krause, T. Klamroth, P. Saalfrank, J. Chem. Phys. **127**, 034107 (2007)
40. P.G. Reinhard, E. Suraud, Ann. Phys. **216**, 98 (1992)
41. E. Suraud, P.G. Reinhard, New J. Phys. **16**, 063066 (2014)
42. L. Lacombe, P.G. Reinhard, P.M. Dinh, E. Suraud, J. Phys. B **49**, 245101 (2016)
43. C. Legrand, E. Suraud, P.G. Reinhard, J. Phys. B **35**, 1115 (2002)
44. P. Klüpfel, P.M. Dinh, P.G. Reinhard, E. Suraud, Phys. Rev. A **88**, 052501 (2013)
45. F. Calvayrac, P.G. Reinhard, E. Suraud, C.A. Ullrich, Phys. Rep. **337**, 493 (2000)
46. P.G. Reinhard, E. Suraud, *Introduction to Cluster Dynamics* (Wiley, New York, 2004)

47. S. Kümmel, M. Brack, P.G. Reinhard, Eur. Phys. J. D **9**, 149 (1999)
48. J.P. Perdew, Y. Wang, Phys. Rev. B **45**, 13244 (1992)
49. B. Montag, P.G. Reinhard, Phys. Lett. A **193**, 380 (1994)
50. B. Montag, P.G. Reinhard, Z. Phys. D **33**, 265 (1995)
51. K.T.R. Davies, S.E. Koonin, Phys. Rev. C **23**, 2042 (1981)
52. M.D. Feit, J.A. Fleck, A. Steiger, J. Comp. Phys. **47**, 412 (1982)
53. V. Blum, G. Lauritsch, J.A. Maruhn, P.G. Reinhard, J. Comp. Phys. **100**, 364 (1992)
54. P.G. Reinhard, P.D. Stevenson, D. Almehed, J.A. Maruhn, M.R. Strayer, Phys. Rev. E **73**, 036709 (2006)
55. R.M. Dreizler, E.K.U. Gross, *Density Functional Theory: An Approach to the Quantum Many-Body Problem* (Springer-Verlag, Berlin, 1990)
56. J. Köhn, R. Redmer, K.H. Meiwes-Broer, T. Fennel, Phys. Rev. A **77**, 033202 (2008)
57. J. Köhn, R. Redmer, T. Fennel, New J. Phys. **14**, 055011 (2012)
58. R. Cusson, P.G. Reinhard, J. Maruhn, W. Greiner, M. Strayer, Z. Phys. A **320**, 475 (1985)
59. C.A. Ullrich, J. Mol. Struct. (THEOCHEM) **501–502**, 315 (2000)
60. P.G. Reinhard, O. Genzken, M. Brack, Ann. Phys. **5**, 1 (1996)
61. J. Babst, P.G. Reinhard, Z. Phys. D **42**, 209 (1997)
62. R. Loudon, *The Quantum Theory of Light* (Oxford Science Publications, Oxford, 2009)
63. L.V. Keldysh, Sov. Phys. J. Exp. Theor. Phys. **20**, 1307 (1965)
64. P.G. Reinhard, F. Calvayrac, C. Kohl, S. Kümmel, E. Suraud, C.A. Ullrich, M. Brack, Eur. Phys. J. D **9**, 111 (1999)
65. B. Montag, P.G. Reinhard, J. Meyer, Z. Phys. D **32**, 125 (1994)
66. M. Brack, Rev. Mod. Phys. **65**, 677 (1993)
67. M. Brack, R.K. Bhaduri, *Semiclassical Physics* (Addison-Wesley, Reading, 1997)